Journal of Materials Chemistry A

Accepted Manuscript

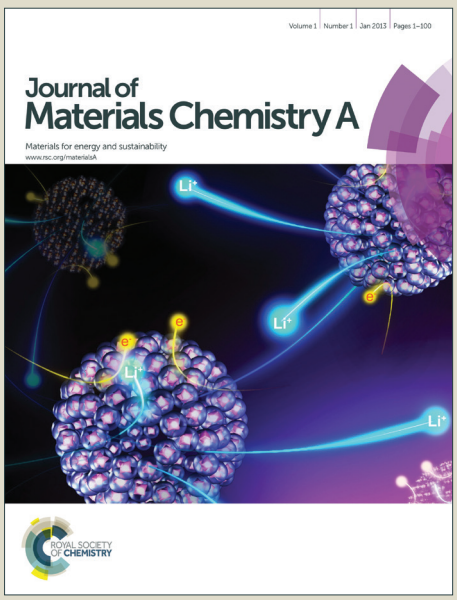

ROYAL SOCIETY OF CHEMISTRY

www.rsc.org/materialsA

Journal of Materials Chemistry A RSCPublishing

ARTICLE

Co–Sb intermetallic compounds and their disproportionated nanocomposites as high-performance anodes for rechargeable Li-ion batteries

Cite this: DOI: 10.1039/x0xx00000x

Received 00th January 2014,
Accepted 00th January 2014

DOI: 10.1039/x0xx00000x

www.rsc.org/

Min-Gu Park[a], Jun Ho Song[b], Jung-Soo Sohn[c], Churl Kyoung Lee*[a] and Cheol-Min Park*[a,d]

Co–Sb intermetallic compounds (CoSb, $CoSb_2$, and $CoSb_3$) were simply synthesized by solid-state synthesis routes and their potential as anode materials for Li-ion batteries was investigated. The $CoSb_3$ electrode showed poor electrochemical behavior, but the CoSb and $CoSb_2$ electrodes showed relatively good electrochemical performance. Additionally, the reaction mechanisms of CoSb, $CoSb_2$, and $CoSb_3$ with Li were identified using ex situ X-ray diffraction. To improve the electrochemical performance of the Co–Sb intermetallic compounds, nanostructured composites of these compounds modified with carbon were prepared using a high-energy mechanical milling technique. Among the fabricated nanocomposites, the $CoSb_2$/C nanocomposite electrode comprising disproportionated nanocrystalline CoSb, amorphous Sb, and an amorphous carbon matrix showed excellent electrochemical properties, such as a high energy density (1st charge: 578 mAh g^{-1}, or ~2895 mAh cm^{-3}), cycling durability over 100 cycles (above 490 mAh g^{-1}, or ~ 2450 mAh cm^{-3}), good initial Coulombic efficiency (~78.1%), and a fast rate capability (1C: 472 mAh g^{-1}, 3C: 415 mAh g^{-1}). These excellent electrochemical properties demonstrated by the $CoSb_2$/C nanocomposite electrode confirm its potential as an alternative anode material for Li-ion batteries.

Introduction

Rechargeable Li-ion batteries are considered the key to fabricating longer lasting portable electronic devices and hybrid electric vehicles because of their good electrochemical performance. Commercial Li-ion batteries are mainly composed of a graphite anode and a $LiCoO_2$ cathode. Although graphite anodes show good electrochemical behavior resulting from Li intercalation, they have a relatively small theoretical capacity of 372 mAh g^{-1} and poor rate capability. Therefore, ongoing research efforts have been focused on achieving high initial Coulombic efficiency, high energy density, long cyclability, and fast rate capability of anodes for Li-ion batteries.[1-15] Among the many candidate elements for high-capacity anode materials; such as Sn, Si, P, and Sb; many studies have been devoted to Sb-based systems because of their relatively high gravimetric (Li_3Sb: 660 mAh g^{-1}) and volumetric capacities (~ 4370 mAh cm^{-3}).[16-34] However, Sb-based systems generally suffer from poor cycling behavior because of the large volume change that occurs during the repeated charge/discharge reactions.

To solve the aforementioned problems, researchers have focused on Sb-based intermetallics or nanocomposite materials as alternative solutions, in order to alleviate the issue of volume change that occurs during cycling. Sb-based intermetallics show an interesting reaction mechanism with Li.[19-34] During the Li insertion reaction in Sb-based intermetallics, M_xSb_y (M = Ti, V, Mn, Fe, Co, Ni, Cu, and Zn with x, y = 1, 2, 3) can form (i) a Li ternary phase through an insertion (or addition) reaction and (ii) an Li_3Sb phase with a nanocrystalline metal by a conversion reaction. The insertion and conversion reactions can be summarized as follows:

Insertion (addition) reaction: $M_xSb_y + zLi \rightarrow Li_zM_xSb_y$ (1)

Conversion reaction: $M_xSb_y + 3yLi \rightarrow yLi_3Sb + xM$ (2)

The formation of $Li_zM_xSb_y$ by insertion reaction (1) results in good electrochemical behavior attributable to stable crystalline structures, which is advantageous for high-performance anode materials.[20,21,32-34] On the other hand, conversion reaction (2) produces a nanocrystalline metal and Li_3Sb, which afford advantageous features in terms of less severe structural stress.[22-31] Although various intermetallic compounds have shown enhanced electrochemical properties, the electrochemical performance of these compounds is still poor, thus preventing their commercial use.

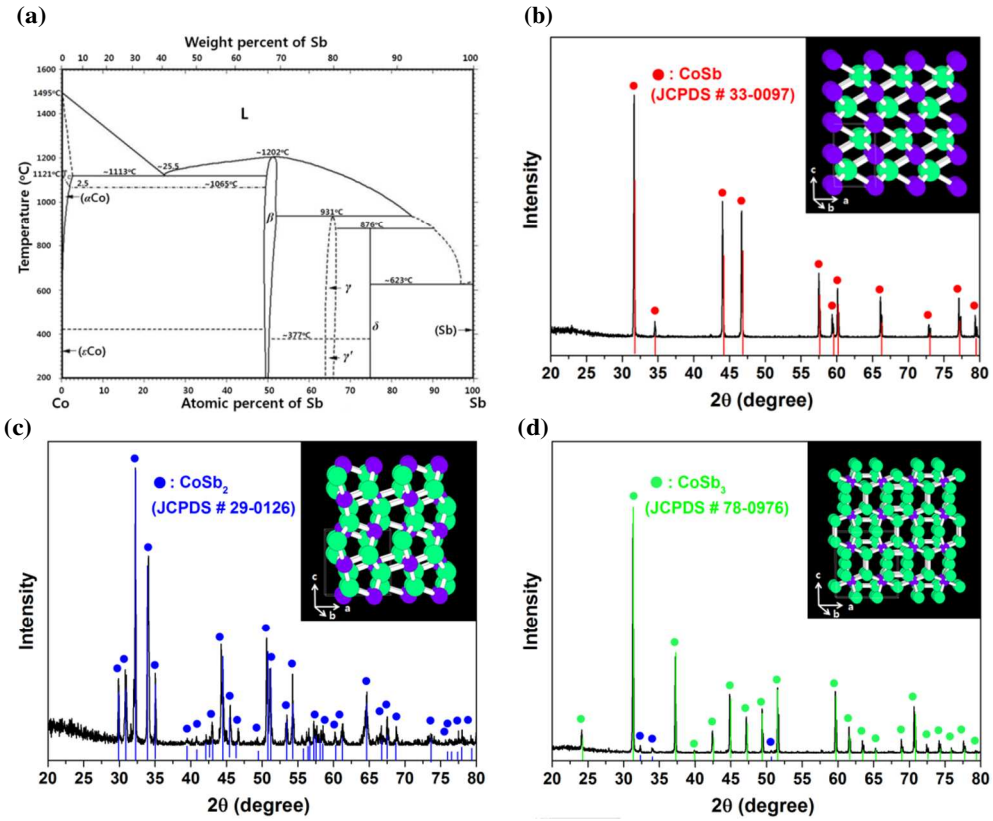

Fig. 1 Phase diagram, XRD patterns, and ball-and-stick models of crystalline structures (Co: purple, Sb: green) of the Co–Sb intermetallic compounds: (a) Co–Sb binary phase diagram and XRD patterns with crystalline structures of (b) CoSb, (c) $CoSb_2$, and (d) $CoSb_3$.

Nanostructured materials are considered another suitable alternative to Li alloy-based electrode materials.[35-37] Because nanostructured materials show full theoretical capacity owing to their large interfacial area, stable cycling behavior is obtained by accommodating the strain generated during cycling and a fast rate capability is accomplished by increasing the Li ion diffusion rate.[38] However, nanosized materials have detrimental effect from their agglomeration during repeated cycling, which results from their high surface reactivity. Nanocomposites modified with carbon are considered to be a practical solution for Li alloy-based anodes because the agglomeration of nanosized metal particles, caused by the high surface reactivity, can be minimized using finely dispersed, nanosized metallic particles in the carbon matrix.[1,14,15,19-23,] Many studies have demonstrated the superior cycling performance of nanocomposite materials. Various methods, such as high-energy mechanical milling (HEMM), co-precipitation, reduction, sol–gel, and so on, have been suggested for producing nanocomposite anodes.[39-44] Among these, the HEMM method is very attractive because it is a simple procedure that can produce nanocomposite powders with fewer impurities, unlike the chemical methods.[42-44] The anode of the Nexelion™ battery, designed and commercialized by Sony in 2005, is mainly composed of an amorphized Sn/Co/C composite synthesized by the HEMM technique.[44]

In this study, we aimed to design a nanocomposite anode having excellent electrochemical properties, including long cycling behavior, good initial Coulombic efficiency, high energy density, and fast rate capability. Bearing in mind both the intermetallic compounds and the nanocomposites modified with carbon, to enhance the electrochemical performances of the Sb, Co-Sb intermetallics (CoSb, $CoSb_2$, and $CoSb_3$) and their nanocomposites were synthesized and tested as anode materials for rechargeable Li-ion batteries. Additionally, the reaction mechanisms of the Co–Sb intermetallics were thoroughly examined during Li insertion/extraction.

Experimental

Co–Sb intermetallic compounds, CoSb, $CoSb_2$, and $CoSb_3$, were synthesized by the following process. Stoichiometric amounts of Co (99.9%, Aldrich) and Sb (99.5%, Aldrich) powders were mixed using HEMM for 1 h and placed in a quartz tube that was heated to 800 °C for 3 h under an Ar atmosphere at a heating rate of 3 °C min^{-1}. Then, the furnace was automatically cooled to room temperature. To produce their corresponding nanostructured composites, CoSb (or $CoSb_2$, $CoSb_3$) and carbon (Super P) were put into a hardened steel vial of capacity 80 cm^3 along with stainless steel balls (diameters: 3/8 in. and 3/16 in.) at a ball-to-powder weight ratio of 20:1. The HEMM process (Spex-8000) was conducted under Ar atmosphere for 12 h. The preliminary electrochemical tests showed that the optimal amounts of CoSb (or $CoSb_2$, $CoSb_3$) and C were 60% and 40% by weight, respectively.

The CoSb, $CoSb_2$, and $CoSb_3$ compounds and their nanocomposites were characterized using X-ray diffractometry (XRD, Rigaku, X-MAX/200-PC) and high-resolution transmission electron microscopy (HRTEM, FEI 20) operating

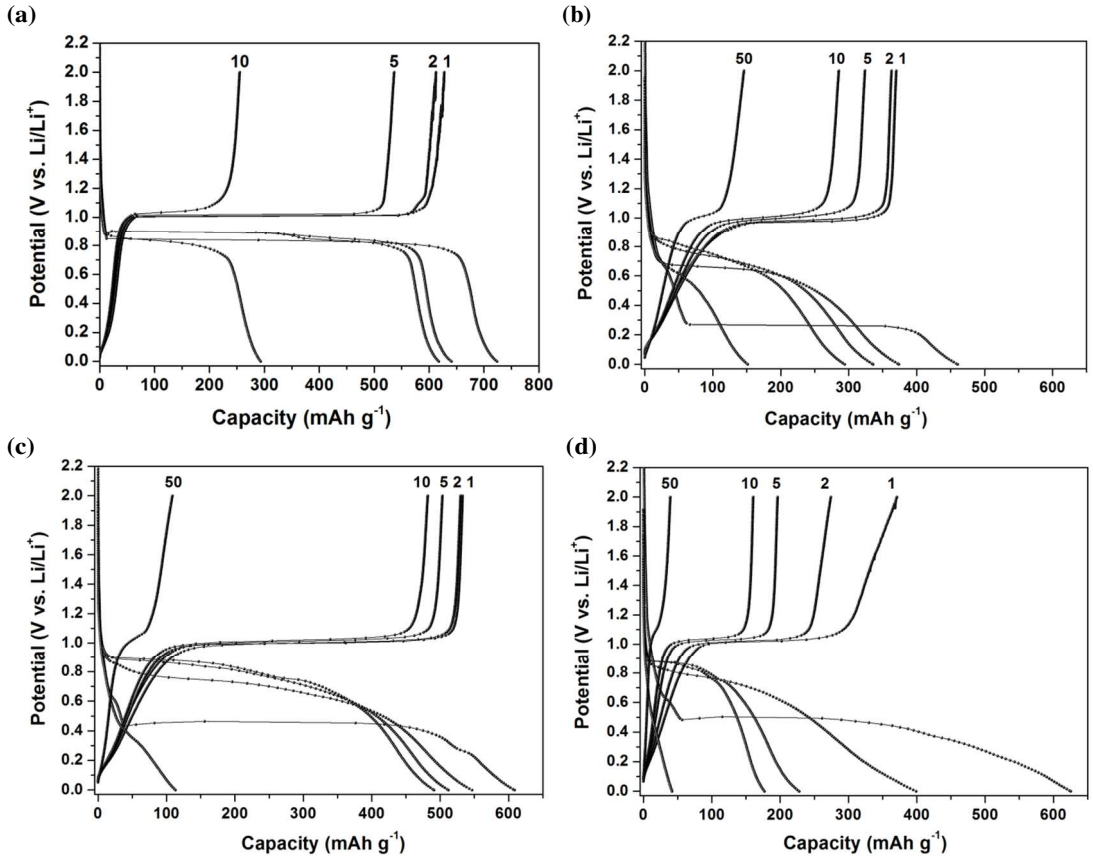

Fig. 2 Voltage profiles for the Co–Sb intermetallic compounds electrodes for the 1st, 2nd, 5th, 10th, and 50th cycles: (a) Sb, (b) CoSb, (c) $CoSb_2$, and (d) $CoSb_3$.

at 200 kV. Ex situ XRD methods were used to observe the structural changes that occurred in the active materials of the CoSb, $CoSb_2$, and $CoSb_3$ electrodes during cycling. The electrodes were detached from the cell, washed with diethylcarbonate (DEC), and coated with Kapton tape, which served as a protective film. For the TEM analyses of the nanocomposites, dilute suspensions of the samples were dropped onto a carbon-coated TEM grid and then allowed to dry. For the electrochemical evaluation of CoSb, $CoSb_2$, and $CoSb_3$, and their corresponding nanocomposites modified using carbon, the electrodes were prepared by coating a slurry containing the active material (70 wt%), carbon black (Denka, 15 wt%) as a conductor, and polyvinylidene fluoride (PVDF) dissolved in N-methyl pyrrolidinone (NMP) as the binder (15 wt%) onto the copper foil substrates. These samples were pressed and dried under vacuum at 120 °C for 3 h (electrode thickness: ~ 0.045 mm, area: 0.79 cm^2, weight of active material: ~ 3.5 mg). Laboratory-made coin-type electrochemical cells were assembled in an Ar-filled glove box using Celgard 2400 as the separator, Li foil as the counter and reference electrodes, and 1 M $LiPF_6$ in ethylene carbonate (EC)/diethyl carbonate (DEC) (1:1 by volume, PANAX Starlyte) as the electrolyte. All of the cells were galvanostatically tested between 0.0 and 2.0 V (vs. Li/Li^+) at a current density of 100 mA g^{-1} using a Maccor automated tester. The gravimetric capacity was calculated with respect to all the elements, whereas the volumetric capacity was obtained from the gravimetric capacity by multiplying the density (CoSb: 8.87 g cm^{-3}, $CoSb_2$: 8.35 g cm^{-3}, $CoSb_3$: 7.64 g cm^{-3}) of the active elements by their weight percent. Li was inserted into the electrode during the discharge reaction and was extracted from the working electrode during the charge reaction.

Results and discussion

Figure 1a shows a Co-Sb phase diagram, which composed of three intermetallic compounds, CoSb, $CoSb_2$, and $CoSb_3$. Figures 1b–d show the XRD patterns of the intermetallic CoSb, $CoSb_2$, and $CoSb_3$, respectively, synthesized by simple solid-state synthetic routes. The XRD patterns of Fig. 1b and c corresponded to the CoSb and $CoSb_2$ phases, respectively; no other crystalline phases were detected. In the case of $CoSb_3$ (Fig. 1d), most of the peaks corresponded to the $CoSb_3$ phase, and small $CoSb_2$ peaks (32.3°, 34.0°, and 50.6°) were detected. The amount of $CoSb_2$ was negligibly small based on the estimation from the X'pert Highscore program (ca. 2%).

The crystalline structures of hexagonal CoSb (JCPDS #33-0097, space group: P63/mmc, a = b = 3.890, c = 5.187, γ = 120°), monoclinic $CoSb_2$ (JCPDS #29-0126, space group: P121/c1, a = 6.508, b = 6.388, c = 6.543, β = 117.66°), and cubic $CoSb_3$ (JCPDS #78-0976, space group: Im-3, a = b = c = 9.0775) are shown in the insets in Figs. 1b–d, respectively. All the crystalline structures contained channels or voids available for facile Li diffusion and storage, which demonstrates that the Co–Sb intermetallics have significant potential for use as anode materials for rechargeable Li-ion batteries.

Table 1 Electrochemical characteristics for Sb, CoSb, $CoSb_2$, and $CoSb_3$ electrodes.

Electrode	1st discharge capacity [mAh g^{-1}]	1st charge capacity [mAh g^{-1}]	Initial coulombic efficiency [%]	Capacity retention after Xth charge capacity [%]
Sb	724	627	86.6	40.7 (X = 10)
CoSb	460	370	80.4	40.1 (X = 50)
$CoSb_2$	609	533	87.5	20.3 (X = 50)
$CoSb_3$	625	371	59.4	10.5 (X = 50)

The voltage profiles of the Sb, CoSb, $CoSb_2$, and $CoSb_3$ electrodes are shown in Figs. 2a–d, respectively. In addition, the first discharge and charge capacities, along with the Coulombic efficiencies for the first cycle and the capacity retentions of the Sb, CoSb, $CoSb_2$, and $CoSb_3$ electrodes, are presented in Table 1. Although the pure Sb electrode exhibited a good initial Coulombic efficiency of 86.6%, the electrode showed very poor capacity retention of 40.7% of the initial charge capacity after the 10th cycle. The drastic decrease in capacity of the Sb electrode was caused by the large volume change due to the formation of Li_3Sb, which is associated with the pulverization of the active material and its electrical isolation from the current collector.[17] The electrochemical reaction mechanism of the Sb electrode with Li showed the successive formation of Li_2Sb (0.82 V) and Li_3Sb (0.8 V) during the discharge reaction.[17] The intermetallic CoSb, $CoSb_2$, and $CoSb_3$ electrodes showed enhanced capacity retentions as compared to the Sb electrode. Among the electrodes, the $CoSb_2$ electrode showed a high initial discharge/charge capacity of 609/533 mAh g^{-1} and a good initial Coulombic efficiency of 87.5%. The $CoSb_3$ electrode showed poor electrochemical behavior, with a low initial Coulombic efficiency of 59.4% and a poor capacity retention of 10.5% of the initial charge capacity after the 50th cycle. Although the CoSb electrode showed a relatively small initial charge capacity of 370 mAh g^{-1}, the electrode showed a good initial Coulombic efficiency of 80.4% and a relatively stable capacity retention of 40.1% after the 50th cycle as compared with the other compound electrodes.

The differential capacity plots (DCP, Fig. 3a) for the first cycle of the CoSb, $CoSb_2$, and $CoSb_3$ electrodes showed a large peak during discharge and charge, respectively. Figures 3b–d present the results of the ex situ XRD analyses of the CoSb, $CoSb_2$, and $CoSb_3$ electrodes, respectively, performed at selected potentials, as indicated in the DCP of Fig. 3a. When the electrodes were fully discharged at 0 V (Figs. 3b-2, 3c-5, 3d-8), the CoSb, $CoSb_2$, and $CoSb_3$ phases disappeared and only Li_3Sb phases appeared, which demonstrates that CoSb, $CoSb_2$, and $CoSb_3$ were transformed to Co and Li_3Sb by conversion reactions. In the fully charged state at 2 V (Figs. 3b-3, 3c-6, 3d-9), amorphization of the DCP peaks was observed. The DCP results of the second discharge reaction showed

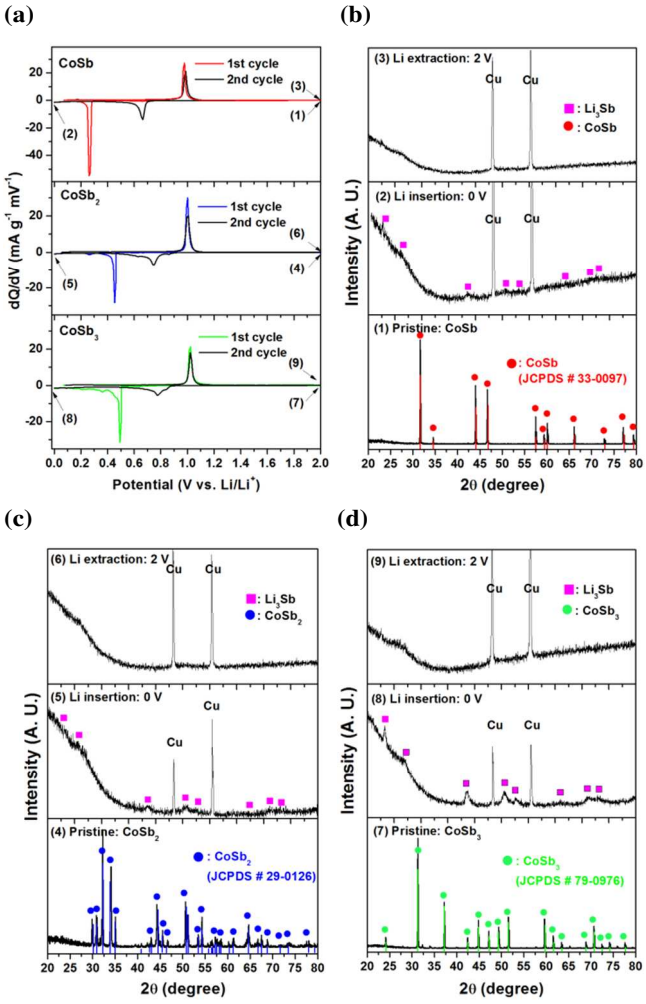

Fig. 3 Reaction mechanisms between Co–Sb intermetallic compounds and Li: (a) DCP results and ex situ XRD results of (b) CoSb, (c) $CoSb_2$, and (d) $CoSb_3$. (Cu: current collector)

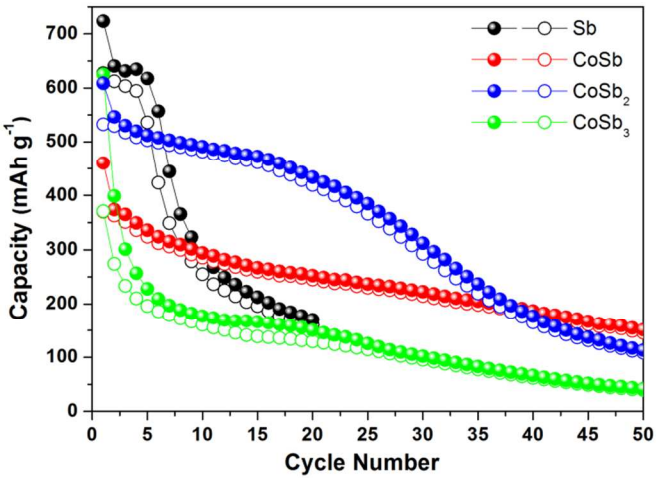

Fig. 4 Comparison of cycle performances for the Sb, CoSb, $CoSb_2$, and $CoSb_3$ electrodes.

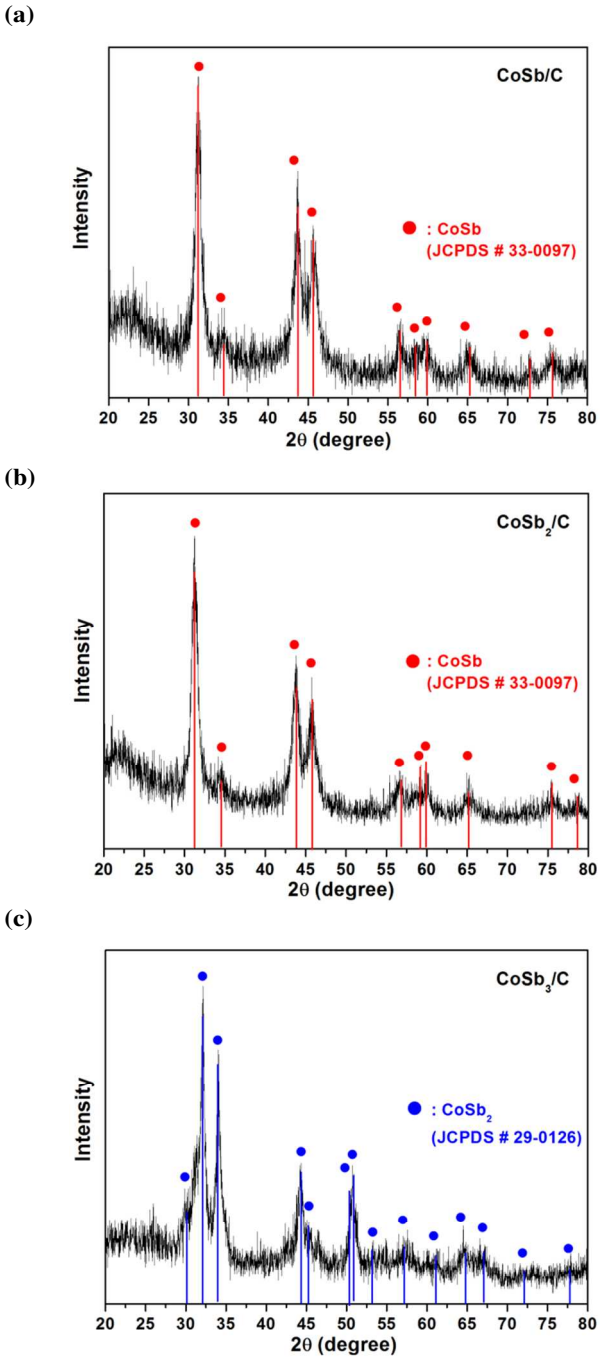

Fig. 5 XRD patterns of the $CoSb_x$/C nanocomposites: (a) CoSb/C, (b) $CoSb_2$/C, and (c) $CoSb_3$/C.

apparent peaks of ~ 0.8 V corresponding to Li–Sb reactions (0.82 V: Sb → Li_2Sb; 0.79 V: Li_2Sb → Li_3Sb), which confirmed that the remaining phases at the fully charged state were Co and Sb. Previous Sb-based intermetallic compound-related studies demonstrated that well-dispersed nanocrystalline metal and Li_3Sb phases are formed at the fully discharged states by the conversion reaction.[24-31] This feature is advantageous for the electrochemical performance in terms of less severe structural stress. Additionally, the DCP peaks near 0.26, 0.45, and 0.49 V during the first discharge reactions of the CoSb, $CoSb_2$, and $CoSb_3$ electrodes, respectively, were lower than the reaction potential of the Sb electrode because the overpotentials of the Co–Sb electrodes caused the break up the Co–Sb bonds though the conversion reaction in order to form the nanocrystalline Li_3Sb and Co phases. On the basis of the above DCP and ex situ XRD results, the reactions involved during the first discharge and charge cycles can be expressed as follows:

During discharge: $CoSb_x$ (x = 1, 2, 3) → Li_3Sb + Co
During charge: Li_3Sb + Co → Sb + Co (amorphization)

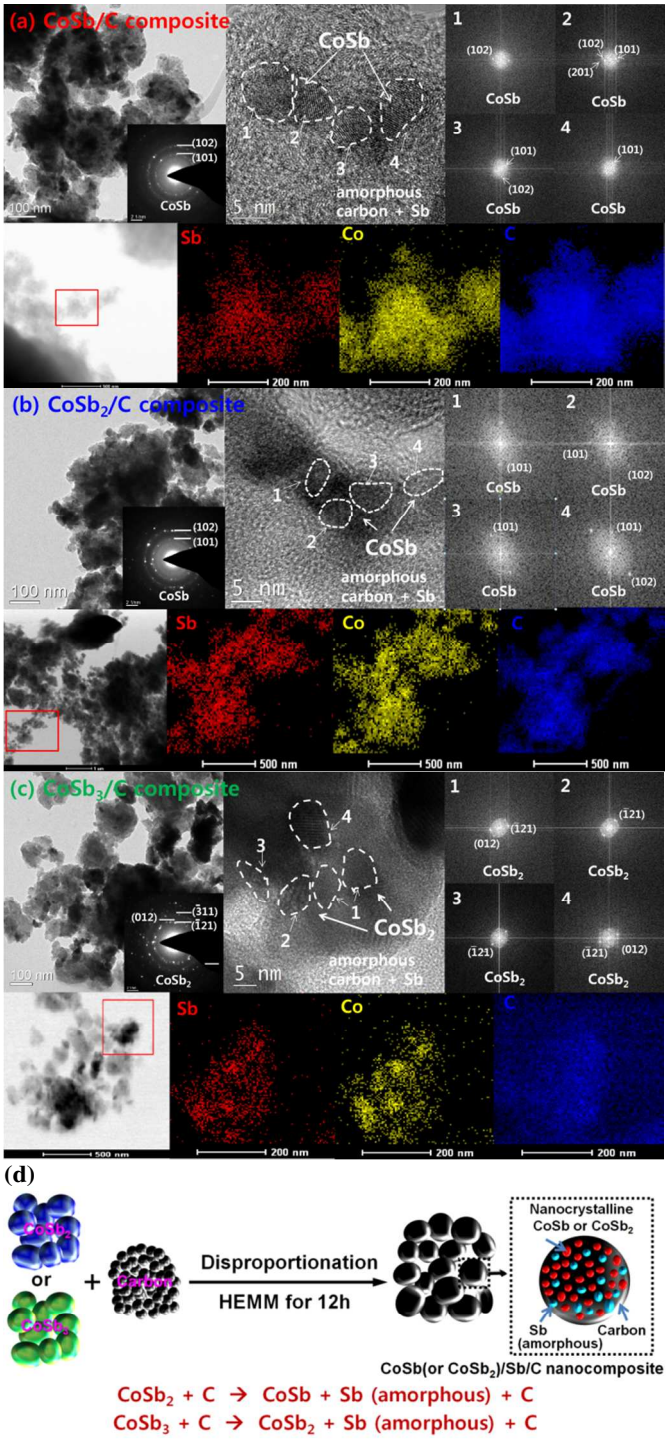

Fig. 6 TEM bright-field, HRTEM images combined with FT patterns, and STEM and its EDS mapping images for the $CoSb_x$/C nanocomposites: (a) CoSb/C, (b) $CoSb_2$/C, (c) $CoSb_3$/C and (d) schematic view of $CoSb_x$/C nanocomposites.

The cycling performance (Fig. 4) for the Sb, CoSb, $CoSb_2$, and $CoSb_3$ electrodes were compared at voltages ranging from 0.0 to 2.0 V and a current rate of 100 mA g^{-1}. The cycling performance of the Sb electrode was very poor. The reversible capacities and capacity retentions of the CoSb, $CoSb_2$, and $CoSb_3$ electrodes were significantly enhanced as compared with the Sb electrode. These enhanced electrochemical characteristics of the CoSb, $CoSb_2$, and $CoSb_3$ electrodes are attributed to the good dispersion of the amorphized Sb and the inactive Co nanocrystallites achieved through the conversion reaction during the first cycle. In terms of the cycling performance, the CoSb electrode was better than the $CoSb_2$ and $CoSb_3$ electrodes, but its capacity decreased gradually with each cycle. On the basis of the electrochemical behaviors of the Co–Sb intermetallic compound electrodes, it can be concluded that the $CoSb_2$ electrode shows high charge capacity, whereas the CoSb electrode shows stable capacity retention.

Nanocomposites produced using the HEMM technique are attractive for the fabrication of high-performance anode materials because this method yields well-distributed, nanosized metal or alloy crystallites in a carbon matrix. In the HEMM technique, the particles undergo plastic deformation, leading to work hardening and fracture upon impact at temperatures above 200 °C and pressures on the order of 6 GPa.[45] Nanocomposites containing carbon, i.e., CoSb/C, $CoSb_2$/C, and $CoSb_3$/C, were prepared using the HEMM technique in order to enhance the electrochemical properties of the Co–Sb intermetallic compounds. The XRD patterns of the CoSb/C, $CoSb_2$/C, and $CoSb_3$/C nanocomposites are shown in Figs. 5a–c, respectively. In Fig. 5a, all the peaks of the XRD pattern of CoSb/C corresponded to the CoSb phase with reduced crystallinity because of the HEMM process. A small broad peak of 20-25° corresponded to milled amorphous carbon. The XRD patterns of the $CoSb_2$/C and $CoSb_3$/C nanocomposites corresponded to only the CoSb and $CoSb_2$ phases with reduced crystallinity, respectively, which demonstrates that the $CoSb_2$ within the $CoSb_2$/C nanocomposite was disproportionated to CoSb and Sb (amorphous) while the $CoSb_3$ within the $CoSb_3$/C nanocomposite was disproportionated to $CoSb_2$ and Sb (amorphous) as a result of the HEMM process. The disproportionation reactions occurred because the CoSb and $CoSb_2$ phases are more thermodynamically stable than the $CoSb_2$ and $CoSb_3$ phases, respectively. A similar disproportionation reaction has also been observed for SiO samples. SiO was disproportionated to nanocrystalline Si and SiO_2 at high temperature.[46-48]

The TEM bright-field, HRTEM images combined with Fourier transformed (FT) patterns, and STEM and its energy dispersive scanning (EDS) mapping images for the CoSb/C, $CoSb_2$/C, and $CoSb_3$/C nanocomposites are given in Figs. 6a–c, respectively. The HRTEM, FT patterns, and EDS mapping images of the CoSb/C nanocomposite (Fig. 6a) show that well-dispersed CoSb nanocrystallites with sizes of approximately 5–10 nm were contained within the amorphous carbon matrix. In Fig. 6b, the HRTEM, FT patterns, and EDS mapping images of the $CoSb_2$/C nanocomposite show that CoSb nanocrystallites approximately 5–10 nm in size and amorphous Sb were well dispersed within the amorphous carbon matrix, which confirmed that the $CoSb_2$ phase was fully disproportionated to nanocrystalline CoSb and amorphous Sb. In the case of the $CoSb_3$/C nanocomposite, the full disproportionation reaction of $CoSb_3$ to nanocrystalline $CoSb_2$ and amorphous Sb, in addition to their good dispersion, were also confirmed by the HRTEM image, FT patterns, and EDS mapping images (Fig. 6c). The disproportionation reactions in the $CoSb_2$/C and $CoSb_3$/C nanocomposites coincided with the XRD results, which is schematically illustrated in Fig. 6d.

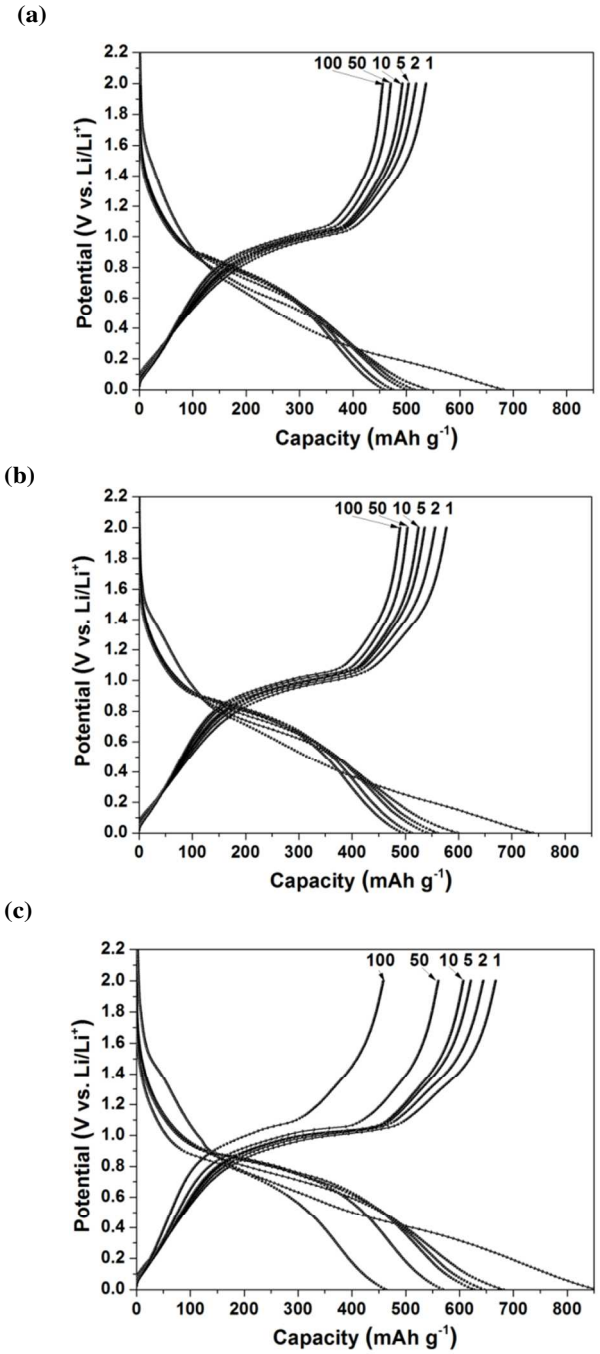

Fig. 7 Voltage profiles for the $CoSb_x$ nanocomposites electrodes for the 1st, 2nd, 5th, 10th, 50th, and 100th cycles: (a) CoSb/C, (b) $CoSb_2$/C, and (c) $CoSb_3$/C nanocomposites.

Table 2 Electrochemical characteristics for CoSb/C, $CoSb_2$/C and $CoSb_3$/C nanocomposite electrodes.

Electrode	1st discharge capacity [mAh g^{-1}]	1st charge capacity [mAh g^{-1}]	Initial Coulombic efficiency [%]	Capacity retention after Xth charge capacity [%]
CoSb/C	682	536	78.6	85.1 (X = 100)
$CoSb_2$/C	740	578	78.1	85.0 (X = 100)
$CoSb_3$/C	854	667	78.1	68.7 (X = 100)

The voltage profiles of the CoSb/C, $CoSb_2$/C, and $CoSb_3$/C nanocomposite electrodes are shown in Figs. 7a–c, respectively. In addition, the first discharge and charge capacities with the Coulombic efficiencies for the first cycle and capacity retentions after the 100th cycle of the nanocomposite electrodes are presented in Table 2. Among the nanocomposite electrodes, the $CoSb_3$/C nanocomposite electrode showed a high initial discharge/charge capacity of 854/667 mAh g^{-1} with a good initial Coulombic efficiency of 78.1%, but the capacity retention after the 100th cycle was poor. The CoSb/C nanocomposite electrode showed a high initial charge capacity of 536 mAh g^{-1} with a good initial Coulombic efficiency of 78.6% and a high capacity retention of 85.1% after the 100th cycle. The $CoSb_2$/C nanocomposite electrode showed a high reversible charge capacity of 578 mAh g^{-1} (~ 2895 mAh cm^{-3}) with a good initial Coulombic efficiency of 78.1% and a high capacity retention of 85.0% after the 100th cycle. The first charge capacity of the $CoSb_2$/C nanocomposite electrode was contributed to the disproportionated CoSb (35.8 wt%; ca. 159 mAh g^{-1}), amorphous Sb (24.2 wt%; ca. 159 mAh g^{-1}), and amorphous carbon (40 wt%; ca. 260 mAh g^{-1}). Among the nanocomposite electrodes, the $CoSb_2$/C nanocomposite electrode showed the best electrochemical performance with high capacity, good initial Coulombic efficiency, and high capacity retention. The good electrochemical performance of the $CoSb_2$/C nanocomposite electrode is attributed to the formation of well-dispersed nanocrystalline CoSb and amorphous Sb within the amorphous carbon matrix by the disproportionation reaction.

The cycling performance of the Sb, CoSb/C, $CoSb_2$/C, and $CoSb_3$/C nanocomposite electrodes were compared at voltages ranging from 0.0 to 2.0 V and a current rate of 100 mA g^{-1}. As shown in Fig. 8, the cycling performance of the Sb electrode was very poor because of the large volume change due to the formation of Li_3Sb. The reversible capacity and capacity retention of the $CoSb_x$/C nanocomposite electrodes were significantly enhanced as compared with the Sb electrode. Among the nanocomposite electrodes, the CoSb/C and $CoSb_2$/C nanocomposite electrodes showed very stable cyclability over 100 cycles. The CoSb/C nanocomposite electrode showed a good initial Coulombic efficiency of 78.6%, a high gravimetric and volumetric capacity of 536 mAh g^{-1} and ~ 2850 mAh cm^{-3}, respectively, and stable cycling behavior. The $CoSb_2$/C nanocomposite electrode also showed a good initial Coulombic efficiency of 78.1%, high gravimetric and volumetric capacity

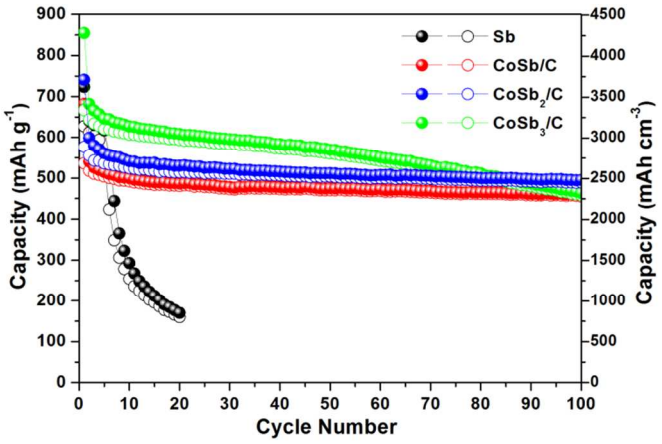

Fig. 8 Comparison of cycle performance for the Sb, CoSb/C, $CoSb_2$/C, and $CoSb_3$/C nanocomposite electrodes.

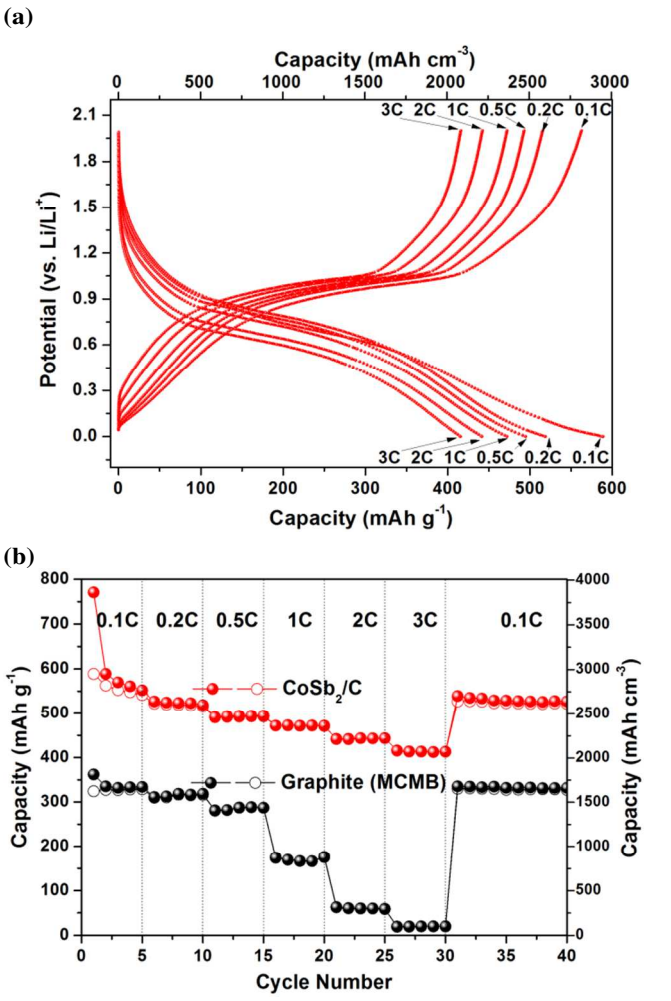

Fig. 9 Comparison of rate capability: (a) voltage profiles at various C rates for $CoSb_2$/C nanocomposite electrode and (b) plot of capacity vs. cycle number of MCMB–graphite and $CoSb_2$/C nanocomposite electrodes at various C rates.

of 578 mAh g^{-1} and ~ 2895 mAh cm^{-3}, respectively, and stable cycling behavior. The CoSb/C and $CoSb_2$/C nanocomposites were composed of nanocrystalline CoSb and disproportionated nanocrystalline CoSb with amorphous Sb, respectively. As confirmed in Fig. 4, the CoSb electrode showed the best cycling behavior among the Co–Sb intermetallic compounds, which contributed to good cycling behavior for the CoSb/C and $CoSb_2$/C nanocomposites. Additionally, several studies have reported that amorphous structured materials showed excellent electrochemical performance. Therefore, it can be stated that the amorphous Sb in the $CoSb_2$/C nanocomposites also contributed to the good cycling performance of the $CoSb_2$/C nanocomposite electrode. Consequently, these good electrochemical characteristics are attributed to the uniform distribution of nanocrystalline CoSb and amorphous Sb within the amorphous carbon matrix by the disproportionation reaction and the conversion reaction of the CoSb phase during Li reactions. The high initial Coulombic efficiency, high capacity, and long cycling behaviour of the $CoSb_2$/C nanocomposite electrode was far better values than those of previous intermetallic Co-Sb based compounds-related studies, such as solvothermally prepared $CoSb_2$,[24,49] template-synthesized CoSb nanowires,[50] carbothermally reduced CoSb,[31] $CoSb_3$-MCMB composite,[30] and so on.[25-29]

The rate capability of the nanocomposite electrodes was also tested, and Figs. 9a and b show the cycling stability of the $CoSb_2$/C nanocomposite as a function of the C rate, with C being defined as the full use of the restricted charge capacity ($CoSb_2$/C: 578 mAh g^{-1}) in 1 h. The $CoSb_2$/C nanocomposite electrode showed excellent rate capability, far better than that of the commercially available MCMB graphite anode, as shown in Fig. 9b. At rates of 1C and 3C, the $CoSb_2$/C nanocomposite electrode showed very high charge capacities of 472 mAh g^{-1} and 415 mAh g^{-1} (or ~ 2360 and 2080 mAh cm^{-3}), respectively, corresponding to 82% and 72%, respectively, of the initial charge capacity with stable cycling behavior. The fast rate capability of the nanocomposite electrodes is attributed to the preparation of the 5–10-nm-sized nanocrystalline CoSb and amorphous Sb by the disproportionation reaction using HEMM.

Conclusions

In the search for suitable anode materials for Li-ion batteries, intermetallic Co–Sb compounds (CoSb, $CoSb_2$, and $CoSb_3$) and their nanostructured composites were synthesized by solid-state synthetic routes. The CoSb/C, $CoSb_2$/C, and $CoSb_3$/C nanocomposite electrodes exhibited better electrochemical behavior as anode materials for rechargeable Li-ion batteries than the Co–Sb intermetallic compound electrodes. Among the nanocomposite electrodes, $CoSb_2$/C showed better electrochemical behavior than the other two nanocomposite electrodes. The $CoSb_2$/C nanocomposite electrode showed a highly reversible reaction with Li, a high charge capacity of 578 mAh g^{-1} or ~ 2895 mAh cm^{-3} with a good initial Coulombic efficiency of 78.1%, cycling durability with a capacity above 490 mAh g^{-1} or 2450 mAh cm^{-3} for over 100 cycles, and fast rate capability with 82% and 72% of the initial charge capacity at 1C and 3C rate, respectively. This improvement was attributed to the good dispersion of disproportionated nanocrystalline CoSb and amorphous Sb within the conducting amorphous carbon matrix and the conversion reaction of CoSb phase during the Li reactions, which alleviated the volume change that occurred during repeated cycling. The excellent electrochemical properties of the $CoSb_2$/C nanocomposite confirmed their potential as alternative anode materials for rechargeable Li-ion batteries.

Acknowledgements

Financial support by a Korea Evaluation Institute of Industrial Technology grant funded by the Korean Government Ministry of Knowledge Economy (no. 10037148) is acknowledged.

Notes and references

[a] Department of Materials and Science Engineering, Kumoh National Institute of Technology, Gumi, Gyeongbuk 730-701, Republic of Korea. E-mail: cklee@kumoh.ac.kr; Fax: +82-54-478-7769; Tel: +82-54-478-7742, E-mail: cmpark@kumoh.ac.kr; Fax: +82-54-478-7769; Tel: +82-54-478-7746

[b] Advanced Batteries Research Center, Korea Electronics Technology Institute, Seongnam, Gyeonggi 463-816, Republic of Korea

[c] Mineral Utilization Convergence Research Center, Korea Institute of Geoscience and Mineral Resources, Daejeon 305-350, Republic of Korea

[d] Outstanding Research Group Program, Convergence Technology Research Institute, Kumoh National Institute of Technology, Gumi, Gyeongbuk 730-701, Republic of Korea

† Footnotes should appear here. These might include comments relevant to but not central to the matter under discussion, limited experimental and spectral data, and crystallographic data.

Electronic Supplementary Information (ESI) available: [details of any supplementary information available should be included here]. See DOI: 10.1039/b000000x/

1 C.-M. Park, J.-H. Kim, H. Kim and H.-J. Sohn, *Chem. Soc. Rev.*, 2010, **39**, 3115.
2 M. Winter, J. O. Besenhard, M. E. Spahr, and P. Novak, *Adv. Mater.*, 1998, **10**, 725.
3 J. Cabana, L. Monconduit, D. Larcher and M. R. Palacin, *Adv. Energy Mater.*, 2010, **22**, E170.
4 P. G. Bruce, B. Scrosati and J.-M. Tarascon, *Angew. Chem. Int. Ed.*, 2008, **47**, 2930.
5 R. Marom, S. F. Amalraj, N. Leifer, D. Jacob and D. Aurbach, *J. Mater. Chem.*, 2011, **21**, 9938.
6 Y. Idota, T. Kubota, A. Matsufuji, Y. Maekawa and T. Miyasaka, *Science*, 1997, **276**, 1395.
7 R. Zhang and M. S. Whittingham, Electrochem. *Solid-State Lett.*, 2010, **13**, A184.
8 C. J. Wen and R. A. Huggins, *J. Electrochem. Soc.*, 1981, **128**, 1181.
9 Y. Yamada, Y. Iriyama, T. Abe and Z. Ogumi, *J. Electrochem. Soc.*, 2010, **157**, A26.
10 M. Yoshio, T. Tsumura and N. Dimov, *J. Power Sources*, 2005, **146**, 10.
11 A. Netz, R. A. Huggins and W. Weppner, *J. Power Sources*, 2003, **119–121**, 95.
12 O. Mao, R. A. Dunlap and J. R. Dahn, *J. Electrochem. Soc.*, 1999, **146**, 405.
13 D. C. S. Souza, V. Pralong, A. J. Jacobson and L. F. Nazar, *Science*, 2002, **296**, 2012.
14 C.-M. Park and H.-J. Sohn, *Adv. Mater.*, 2007, **19**, 2465.
15 C.-M. Park and H.-J. Sohn, *Chem. Mater.*, 2008, **20**, 6319.
16 J. Wang, I. D. Raistrick and R. A. Huggins, *J. Electrochem. Soc.*, 1986, **133**, 457.
17 C.-M. Park, S. Yoon, S.-I. Lee, J.-H. Kim, J.-H. Jung and H.-J. Sohn, *J. Electrochem. Soc.*, 2007, **154**, A917.
18 A. Dailly, J. Ghanbaja, P. Willmann and D. Billaud, *Electrochim. Acta*, 2003, **48**, 977.
19 C.-M. Park and H.-J. Sohn, *Electrochim. Acta*, 2009, **54**, 6367.
20 C.-M. Park and H.-J. Sohn, *Adv. Mater.*, 2010, **22**, 47.

21 J.-O. Lee, J.-U. Seo, J. H. Song, C.-M. Park and C. K. Lee, *Electrochem. Commun.*, 2013, **28**, 71.
22 C.-M. Park, Y. Hwa, N.-E. Sung and H.-J, Sohn, *J. Mater. Chem.*, 2010, **20**, 1097.
23 C.-M. Park and H.-J. Sohn, *Electrochim. Acta*, 2010, **55**, 4987.
24 J. Xie, X. B. Zhao, G. S. Cao, Y. D. Zhong, M. J. Zhao and J. P. Tu, *Electrochim. Acta*, 2005, **50**, 1903.
25 I. Devos, M. Womes, M. Heilemann, J. Olivier-Fourcade, J.-C. Jumas and J. L. Tirado, *J. Mater. Chem.*, 2004, **14**, 1759.
26 J. Xie, X. Zhao, G. Cao, Y. Zhong and M. Zhao, *J. Electroanal. Chem.*, 2003, **542**, 1.
27 J. Zhu, T. Sun, J. Chen, W. Shi, X. Zhang, X. Lou, S. Mhaisalkar, H. H. Hng, F. Boey, J. Ma and Q. Yan, *Chem. Mater.*, 2010, **22**, 5333.
28 J.-M. Tarascon, M. Morcrette, L. Dupont, Y. Chabre, C. Payen, D. Larcher and V. Pralong, *J. Electrochem. Soc.*, 2003, **150**, A732.
29 R. Alcantara, F. J. Fernandez-Madrigal, P. Lavela, J. L. Tirado, J. C. Jumas and J. Olivier-Fourcade, *J. Mater. Chem.*, 1999, **9**, 2517.
30 L. J. Zhang, X. B. Zhao and D. G. Xia, *Mater. Lett.*, 2005, **59**, 3448.
31 J. Yang, M. Wang, Y. Zhu, H. Zhao, R. Wang and J. Chen, *J. Alloys Compd.*, 2011, **509**, 7657.
32 J. T. Vaughey, J. O′Hara and M. M. Thackeray, *Electrochem. Solid-State Lett.*, 1999, **3**, 13.
33 L. M. L. Fransson, J. T. Vaughey, K. Edstrom and M. M. Thackeray, *J. Electrochem. Soc*., 2003, **150**, A86.
34 L. M. L. Fransson, J. T. Vaughey, R. Benedek, K. Edstrom, J. O. Thomas and M. M. Thackeray, *Electrochem. Commun*., 2001, **3**, 317.
35 A. S. Arico, P. Bruce, B. Scrosati, J.-M. Tarascon and W. V. Schalkwijk, *Nat. Mater*., 2005, **4**, 366.
36 P. Poizot, S. Laruelle, S. Grugeon, L. Dupont and J.-M. Tarascon, *Nature*, 2000, **407**, 496.
37 C. K. Chan, H. Peng, G. Liu, K. Mcilwrath, X. F. Zhang, R. A. Huggins and Y. Cui, *Nat. Nanotechnol.*, 2008, **3**, 31.
38 H. Gleiter, *Prog. Mater. Sci.*, 1989, **33**, 223.
39 M.-S. Park, S. A. Needham, G.-X. Wang, Y.-M. Kang, J.-S. Park, S.-X. Dou and H.-K. Liu, *Chem. Mater.*, 2007, **19**, 2406.
40 C.-M. Park and K.-J. Jeon, *Chem. Commun.*, 2011, **47**, 2122.
41 K. T. Nam, D.-W. Kim, P. J. Yoo, C.-Y. Chiang, N. Meethong, P. T. Hammond, Y.-M. Chiang and A. M. Belcher, *Science*, 2006, **312**, 885.
42 K. T. Lee, Y. S. Jung and S. M. Oh, *J. Am. Chem. Soc*., 2003, **125**, 5652.
43 C. Kim, M. Noh, M. Choi, J. Cho and B. Park, *Chem. Mater.*, 2005, **17**, 3297.
44 H. Ishihara, S. Mizutani and H. Inoue, *US Patent*, Pub. No. US 2006/0115734(2006); <http://www.sony.net/SonyInfo/News/Press/ 200502/05-006E/index.html>.
45 C. Suryanarayana, *Prog. Mater. Sci.*, 2001, **46**, 1.
46 C.-M. Park, W. Choi, Y. Hwa, J.-H. Kim, G. Jeong and H.-J. Sohn, *J. Mater. Chem*., 2010, **20**, 4854.
47 M. Mamiya, M. Kikuchi and H. Takei, *J. Cryst. Growth*, 2002, **237**, 1909.
48 M. Mamiya, H. Takei, M. Kikuchi and C. Uyeda, *J. Cryst. Growth*, 2001, **229**, 457.
49 J. Xie, G. S. Cao, X. B. Zhao, Y.D. Zhong and M. J. Zhao, *J. Electrochem. Soc.*, 2004, **151**, A1905.
50 Y.-W. Yang, F. Liu, T.-Y. Li, Y.-B. Chen, Y.-C. Wu and M.-G. Kong, *Scripta Mat.*, 2012, **66**, 495.